* Most of the materials are from the following paper : Yang, M.-J. and R. A. Houze, Jr., 1996: Momentum budget of a squall line with trailing stratiform precipitation: Calculations with a high-resolution numerical model. J. Atmos. Sci., 53, 3629-3652.

Momentum Budget and Transport of a Squall Line with Trailing Stratiform Precipitation: A GCM Prospective

Ming-Jen Yang
Research and Development Center
Central Weather Bureau

Abstract

In this paper, we investigate the momentum budget of a squall line with trailing stratiform precipitation by examining how the momentum balance varies with respect to the storm's internal structure. In particular, we determine differences between the momentum budgets of the convective and stratiform precipitation regions, which are physically distinct parts of the storm. We use the results from a high-resolution nonhydrostatic numerical simulation of the two-dimensional segment of the 10-11 June 1985 PRE-STORM squall line. The momentum equation is averaged over a 300-km-wide large-scale area for time periods of 1 h. On the 1-h time scale, the standing-eddy and mean-flow circulations account for most of the momentum flux on this time scale.

Because the standing-eddy circulation and the pressure-gradient acceleration vary from one part of the storm to another, the interplay of forces leading to the large-scale momentum tendency also differs strongly from one subregion to another. The convective precipitation region dominates the momentum budget at low levels, where the standing-eddy flux convergence produces a forward acceleration that slightly outweighs the rearward pressure-gradient acceleration. At midlevels, both the convective and stratiform precipitation regions contribute to the net large-scale momentum tendency. The pressure-gradient forces in the convective and stratiform precipitation regions are both strong but oppositely directed; however, the rearward standing-eddy flux convergence in the convective precipitation region is also strong; thus the net large-scale momentum tendency at midlevels is rearward. At upper levels, the momentum budget is completely dominated by the stratiform precipitation region, where a strong forward-directed pressure-gradient acceleration dominates the net large-scale momentum tendency.

These differences between the momentum budgets of the convective and stratiform precipitation regions suggest that rather different large-scale momentum tendencies can arise as a function of storm structure; storms with strong convective precipitation regions and weak stratiform precipitation regions would produce momentum tendencies quite different from storms with well-developed stratiform precipitation regions.

1. Introduction

In the 70's, atmospheric scientists started to recognize the importance of vertical momentum transport by deep convection in large-scale dynamics (for example, Schneider and Lindzen 1976, Stevens et al. 1977, and many others). The traditional thinking was then that convective clouds would transport momentum in a "downgradient" sense, reducing the wind shear of mean flow as predicted by the mixing-length theory. However, Moncrieff (1981) in his theoretical study showed that organized deep convective systems (like squall lines) could transport momentum in a "countergradient" sense, increasing the wind shear of large-scale mean flow. This countergradient momentum transport associated with organized deep convection should be accounted for in cumulus parameterization schemes in large-scale numerical models.

Observations of tropical squall lines showed that the vertical flux of horizontal momentum could be countergradient in the cross-line direction and downgradient in the along-line direction (LeMone 1983; LeMone et al. 1984). The mesoscale modeling study of Gao et al. (1990) and the observational study of Gallus and Johnson (1992) obtained a similar result for a midlatitude squall line (the 10-11 June 1985 PRE-STORM squall line).

The quasi-two-dimensional squall-line prototype idealized by Moncrieff (1992) describes well the overall dynamics of squall lines with leading-line/trailing stratiform structure; however, it leaves unaddressed certain details of the microphysical-dynamical interactions. In such cases, a rapidly moving line of intense convective cells is followed by a region of stratiform precipitation. The convective and stratiform precipitation regions are distinct both kinematically (Houze 1982, 1989) and microphysically (Houze 1989, 1993), and the large-scale flow responds fundamentally differently to the vertical heating profiles in these two regions (Mapes and Houze 1995). The radar echo structure in the convective and stratiform precipitation regions is also distinct, as a result of the different kinematics and microphysics, and techniques are available to separate the convective and stratiform precipitation regions

based on their different reflectivity structure (Churchill and Houze 1984; Steiner et al. 1995).

Until now, the separate roles of the convective and stratiform precipitation regions have not been investigated in terms of how they may influence the large-scale horizontal momentum field. The objective of this study is thus to investigate the momentum budget of a two-dimensional squall line with leading-line/trailing-stratiform structure and thereby gain insight into the contributions of the convective and stratiform precipitation regions to the momentum transports over a large-scale region containing the storm.

To achieve this objective, we make use of the numerical simulation results of Yang and Houze (1995a, b). Their simulation is for the 10-11 June 1985 squall line in PRE-STORM (Johnson and Hamilton 1988; Rutledge et al. 1988; Zhang et al. 1989; and many others). The two-dimensional portion of the storm was identified by Biggerstaff and Houze (1993), who constructed a composite analysis of the Doppler radar data in a 60-km wide strip across the north-central portion of the storm where both the reflectivity and horizontal flow patterns appeared to be the most nearly two-dimensional. Yang and Houze (1995a) verified their model calculations by comparing the analyses of Biggerstaff and Houze (1993) and showed that the model describes reasonably well the portion of the squall line that exhibited the highest degree of two-dimensionality. To the north and south of the quasi-two-dimensional region of the storm, the squall line displayed strongly three-dimensional circulations, which require three-dimensional models and consideration of Coriolis effects (Zhang et al. 1989; Skamarock et al. 1994). In the present study, we do not pursue these broader three-dimensional features. Rather, we extend the study of the two-dimensional aspects of squall systems by examining the momentum budget and transports of the two-dimensional region.

2. Momentum transport

a. Formulation of momentum flux

We define means and perturbations of a velocity component V (V = u or w) as

$$V = \overline{V} + V' \tag{1}$$

and

$$V = [V] + V^{*} \tag{2}$$

where the temporal-average operator is defined as

$$\overline{(\ )} \equiv \frac{1}{T}\int_{T_1}^{T_2} (\ )\,dt \tag{3}$$

and the spatial-average operator is defined as

$$[(\ )] \equiv \frac{1}{L}\int_{0}^{L} (\ )\,dx \tag{4}$$

In (3) and (4), T = 1 h for each of the three lifecycle (initial, mature, and slowly decaying) stages of the storm, and L = 300 km for the large-scale area A (the fine-mesh computational domain) in which the storm is embedded. Following Priestly (1949) for the decomposition of large-scale heat fluxes in general circulations, we decompose the total vertical flux of storm-relative horizontal momentum $\rho_o\left[\overline{u_s w}\right]$ into three physically distinct parts,

$$\underset{T_{tot}}{\rho_o\left[\overline{u_s w}\right]} = \underset{S_m}{\rho_o\left[\overline{u_s}\right]\left[\overline{w}\right]} + \underset{S_e}{\rho_o\left[\overline{u_s}^{*}\,\overline{w}^{*}\right]} + \underset{T_e}{\rho_o\left[\overline{u_s' w'}\right]} \tag{5}$$

where u_S is the storm-relative horizontal wind, w is the vertical velocity, ρ_o is the basic-state density, $\rho_o\left[\overline{u_s}\right]\left[\overline{w}\right]$ is the momentum transport by steady mean flow (S_m), $\rho_o\left[\overline{u_s}^{*}\,\overline{w}^{*}\right]$ is the transport by standing eddies (S_e), and $\rho_o\left[\overline{u_s' w'}\right]$ is the transport by transient eddies (T_e). The steady mean flow represents the mean flow across the 300-km large-scale area; standing eddies comprise the steady-state mesoscale circulation, while the transient eddies are the temporally fluctuating convective-scale flow.

b. Weak transient eddies

Model output also verifies that over the large-scale domain of width L = 300 km, the temporal fluctuations of u_S and w are only weakly correlated on the 1-h time scale. Figure 1, which shows the vertical profiles of each of the terms in (5), illustrates this result: the term T_e in (5) is much smaller than either S_m or S_e. Similar results were found by Caniaux et al. (1995) for a tropical west African squall line with a broad trailing-stratiform precipitation region (see their Figs. 19 and 20). This result means that the 1-h averaged velocity field in the simulated storm thus behaves *as if* the storm were in a steady state. This result indicates that on the 1-h time-scale, the steady-state two-dimensional idealization of Moncrieff (1992) applies to the simulated two-dimensional storm, even though we made no a priori assumption of steady-state conditions.

c. Negative momentum flux

It is shown in Fig. 1 that the total momentum flux T_{tot} is negative at all levels, and so are each of the components S_m, S_e, and T_e. All of the fluxes are transporting front-to-rear (FTR) momentum upward or rear-to-front (RTF) momentum downward. At upper levels (z > 6.5 km), most of the momentum is transported by steady mean flow (S_m curve). Figure 2 shows the wind vectors of domain-averaged

mean flow ($[\overline{u_s}]$ and $[\overline{w}]$; Fig. 2a), standing eddy ($\overline{u_s}^*$ and $\overline{w}^*$; Fig. 2b), and total wind ($\overline{u_s}$ and $\overline{w}$; Fig. 2c) during the mature stage. Mean FTR flow combines with mean upward motion across the whole domain (Fig. 2a). The transport by standing eddies (curve Se in Fig. 1) accounts for most of the total momentum transport at lower-to middle levels ($z < 6.5$ km). The mesoscale circulation shows clearly in the standing-eddy wind field (Fig. 2b), in which the upward branch contains FTR flow, while the downward branch consists primarily of the sloping RTF flow.

d. Vertical convergence of momentum flux

Moncrieff (1992) and LeMone and Moncrieff (1994) work with the combined flux T_{tot}. They idealize the combined mean and eddy flow (Fig. 2c) in terms of three flow branches (rear overturning current, jump updraft, and overturning updraft). Using these three flow branches, Moncrieff (1992) shows that the vertical convergence of the momentum flux is given by,

$$-\frac{1}{\rho_o}\frac{\partial}{\partial z}\left(\rho_o\left\langle\overline{u_s}\,\overline{w}\right\rangle\right) = \frac{1}{L_m}\left(\overline{u_s}^2+\frac{\overline{p_m}}{\rho_o}\right)\Bigg|_0^{L_m} \qquad (6)$$

where

$$\left\langle\left(\ \right)\right\rangle = \frac{1}{L_m}\int_0^{L_m}\left(\ \right)dx \qquad (6A)$$

L_m is the dynamical scale of the mesoscale convective system, and P_m is the pressure in the mesoscale convective system. Equation (6) states that the vertical convergence of the total momentum flux at a given altitude must be accounted for by the net change of kinetic energy plus enthalpy (per unit mass) across the system---*if the system is indeed two-dimensional and steady state.*

Let us assume that the dynamical scale of the system L_m is, in our case, identical to the fine-mesh domain width L (300 km). Then the averaging operators defined in (4) and (6A) are identical. Neglecting T_e in (5), we can rewrite (6) with the aid of (5) as

$$-\frac{1}{\rho_o}\frac{\partial}{\partial z}T_{tot} \approx -\frac{1}{\rho_o}\frac{\partial}{\partial z}(S_m + S_e) \approx \frac{1}{L_m}\left(\overline{u_s}^2+\frac{\overline{p_m}}{\rho_o}\right)\Bigg|_0^{L_m} \qquad (6B)$$

As a further test of whether our 1-h average model calculations are consistent with Moncrieff's (1992) steady-state theory, we calculate the left and right sides of (6B) from model outputs and see if we obtain the same result. The left-hand side of (6B) is plotted in Fig. 3a and the right-hand side in Fig. 3b, for three stages of squall-line development. The two sets of curves are virtually identical. Thus, the vertical convergence of total momentum flux for the time-averaged numerical simulation results could be represented in terms of the change of kinetic energy plus enthalpy across the system, as advocated by Moncrieff (1992) and LeMone and Moncrieff (1994).

The idealization of Moncrieff (1992) seems to fit the present simulation very well. However, when the calculations are filtered to a 1-h time scale, it may not fit so well under slightly more general temporal or spatial conditions. At a smaller time scale, T_e becomes larger, and the idealization cannot be applied. Also, the simulation in this study is verified against the data for *only* the portion of the 10-11 June squall line that exhibited the most ideal two-dimensional structure within the larger system (Biggerstaff and Houze 1993). In portions of the storm better described by three-dimensional dynamics (Skamarock et al. 1994), the momentum budget may have different characteristics and the two-dimensional idealization should be used with appropriate caveats and caution.

3. Momentum budget

The horizontal momentum equation in a coordinate system moving with the squall line can be written as,

$$\underbrace{\frac{\delta u_s}{\delta t}}_{\text{TEN}} = \underbrace{\frac{\partial u_s}{\partial t}}_{} + \underbrace{c\frac{\partial u_s}{\partial x}}_{} = \underbrace{-c_p\theta_{vo}\frac{\partial \pi}{\partial x}}_{\text{PGF}} \underbrace{-u_s\frac{\partial u_s}{\partial x}}_{\text{HAD}} \underbrace{-w\frac{\partial u_s}{\partial z}}_{\text{VAD}} + \underbrace{D_u}_{\text{TRB}} \qquad (7)$$

where c is the storm propagation speed, x and z are the horizontal and vertical coordinates, respectively; TEN is the local derivative (or tendency) in the moving coordinate system, c_p is the specific heat at constant pressure, θ_{vO} is the basic-state virtual potential temperature, π is the nondimensional pressure perturbation, and D_u is the subgrid-scale turbulent mixing. A detailed derivation of Eq. (7) is given in Klemp and Wilhelmson (1978). Terms on the right-hand side of (7) are the pressure-gradient force (PGF) per unit mass, horizontal advection (HAD), vertical advection (VAD), and subgrid-scale turbulence (TRB). Note that the Coriolis force is not included.

For better understanding each subregion's contribution to the momentum budget of the large-scale area A, we can rewrite the momentum equation in a flux form. Combining (7) with the anelastic mass continuity equation, applying the spatial averaging operator (4) over the large-scale domain length L, applying the temporal averaging operator (3) over the time period T, neglecting the turbulence term D_u, ignoring the transient eddy term T_e in (5), and substituting (5) into (7) leads to the time- and space-averaged momentum equation,

$$\left[\frac{\delta \overline{u}_s}{\delta t}\right] \approx -\left[\overline{c_p \theta_{vo} \frac{\partial \pi}{\partial x}}\right] - \left[\frac{\partial}{\partial x}(\overline{u}_s^2)\right] - \frac{1}{\rho_o}\frac{\partial}{\partial z}S_m - \frac{1}{\rho_o}\frac{\partial}{\partial z}S_e \quad (8)$$

TEN PGF HMF VMF VEF

The term on the left of (8) is net momentum tendency (TEN), and terms on the right of (8) are the horizontal pressure-gradient force (PGF), horizontal mean-flow flux convergence (HMF), vertical mean-flow flux convergence (VMF), and vertical eddy-flux convergence by standing eddies (VEF), respectively. Note from (6B) that the last two terms in (8) combine to form Moncrieff's (1992) total flux convergence, which may be expressed in terms of the kinetic energy and enthalpy difference across the system—in the special conditions that apply in this case.

We will see in Fig. 4 that the primary terms determining the large-scale momentum tendency TEN are the pressure gradient force PGF and the combined effects of the vertical flux convergence (VMF+VEF). We will also see that over the system as a whole, PGF and (VMF+VEF) tend to oppose each other. Indeed, in a steady-state system of the type idealized by Moncrieff (1992), these two effects exactly balance over the system as a whole (in the absence of horizontal flux convergence). In an evolving large-scale momentum field, it is the slight imbalance between these two effects that determine how the momentum field changes.

Figure 4 summarizes the momentum balance over a 300-km-wide large-scale area containing the simulated squall-line system. The region is partitioned into four horizontal regions (convective precipitation area, stratiform precipitation area, rear and forward anvil regions) and into three broad altitude layers. In the lowest layer (0–4 km) and upper levels (10–14 km), the net momentum tendency (shown in Fig. 4b) is positive (increasing RTF flow), while at midlevels (4–10 km), the net tendency is negative (increasing FTR flow).

The arrows in Fig. 4a show how much each of the processes represented by the terms on the right-hand side of Eq. (8) contributes to the net momentum tendency in Fig. 4b, according to altitude and subregion of the storm. The strongest contributions are from the convective and stratiform precipitation zones. The arrows show, however, that no single process or any one subregion of the storm dominates the net momentum tendency over the large-scale area. The contribution from the convective precipitation region dominates at low levels, both convective and stratiform precipitation regions contribute significantly to net momentum tendency at midlevels, and the contribution from the stratiform precipitation region is essential at upper levels.

Figure 4a clearly illustrates that the net momentum tendency over the large-scale area is the result of competing processes; *the net momentum tendencies are a delicate imbalance of strong terms of opposite sign.* In particular:

- At low levels (0–4 km), the convective precipitation region alone determines the net momentum tendency on the large scale. The net RTF tendency (Fig. 4b) is the result of a competition of two strong but oppositely directed processes in the convective precipitation region (Fig. 4a). The forward-directed tendency by the standing-eddy flux convergence, which in accordance with its sloping structure transports low-level (midlevel) FTR (RTF) momentum upward (downward) in the convective updrafts (downdrafts), slightly outweighs the rearward-directed pressure-gradient tendency produced by the meso-g-scale low under the sloping updrafts.
- At midlevels (4–10 km), all four subregions contribute significantly to the net tendency (Fig. 4b); the largest forces, however, occur in the convective and stratiform precipitation regions. The net tendency at midlevels (Fig. 4b) is FTR. The pressure-gradient tendencies (FTR in the convective region and RTF in the stratiform region) are both quite strong. In this case, they tend to cancel each other out so that the pressure-gradient acceleration contributes very little to the total tendency at midlevels. However, if the stratiform region were less well developed and the convective region were still strong, the pressure-gradient acceleration in that region might be weaker, leading to a net forward acceleration. Another strong process at midlevels is the vertical eddy-flux convergence in the convective region, which contributes a strong net FTR tendency; the eddy-flux convergence combines with the pressure gradient acceleration in the convective region to overwhelm the RTF pressure-gradient acceleration in the stratiform region, yielding the net FTR tendency in the midlevels (Fig. 4b). Vertical flux by the mean flow is not negligible at these levels, and the forward and rear anvils also make minor but not negligible contributions to the net tendency.
- At upper levels (10–14 km), the convective region (Fig. 4a) contributes very little to the overall momentum tendency (Fig. 4b). The dominant process is the RTF tendency in the stratiform region produced by the mesohigh aloft centered at 12 km.

4. Conclusions

In this paper, we consider the role of the squall-line system in the large-scale budget of momentum. This problem is posed by considering a large horizontal area of which the squall system occupies a subregion. One may think of this area as the grid area of a general circulation model or as a region surrounded by an array of rawinsondes. Such a region may contain a population of clouds, of which a squall line with trailing stratiform precipitation region is one member. To represent the role of the cloud population in the mean conditions over such an area, the standard approach adopted in this study is to perform averaging over the region and let the cloud properties be represented as deviations from the averages of kinematic, thermodynamic, and microphysical variables. In our 2D framework, we let the fine-mesh domain play the role of the large-scale area. It is 300 km across and contains the squall system as well as surrounding anvil regions. This large-scale region contains a cloud population of only one member—the squall line with a trailing stratiform precipitation region.

When the momentum equation is written in flux form, by combining it with the continuity equation and averaging over a large-scale area of horizontal width of 300 km and a time period of 1 h, we obtain terms involving the fluxes by the mean flow and eddy motion. Decomposition of total momentum flux into three physically distinct modes—transports by steady mean flow, standing eddies, and transient eddies—shows that in the middle to upper levels, the transport by steady mean flow contributes most of the total momentum flux. The transport by standing eddies explains most of the total momentum flux in low to middle levels. Transport by transient eddies is negligible. The dominance of momentum transport by two-dimensional steady-state circulation (mean flow plus standing eddies) shows that the 1-h averaged model simulation, and by inference the two-dimensional north-central segment of the 10-11 June squall line system itself, conform to Moncrieff's (1992) analytic idealization of a two-dimensional steady-state squall line. To what extent this idealization may be extended to the whole mesoscale convective system (as modeled by Skamarock et al. 1994) or to the broader population of mesoscale convective systems (as described by Houze et al. 1990) remains to be determined.

The computation results show that the large-scale momentum tendency produced by a squall line with a trailing-stratiform precipitation region are a strong function of the internal structure of the storm. Figure 4a conveys that the locus of the most active processes (as measured by the general length of the arrows) slopes rearward from low levels in the convective precipitation region to the upper levels in the stratiform precipitation region. These arrows show that all the terms in Eq. (8) are significant, and all of the subregions (horizontal and vertical) of the storm contribute rather differently to the net momentum tendency. The contributions by vertical standing-eddies flux convergence and by pressure-gradient forces attains the largest magnitudes; however, they tend to work in opposite directions, so that the resulting net momentum tendency is a small residual between these large terms, which behave differently from one region of the storm to another. It seems clear that *storm structure can influence the nature of the net momentum tendency on the large scale*; a storm dominated by a strong convective precipitation region could well produce a very different net large-scale momentum tendency than a storm with strong stratiform precipitation region and a weak convective precipitation region. Techniques to distinguish convective and stratiform precipitation regions from radar data (e.g., Steiner et al. 1995) may prove useful in this respect.

Thus, there appear to be no short cuts to the parameterization of momentum tendencies produced by mesoscale convective systems. Except for transient eddies, which do not produce a strong effect, all the processes of momentum generation and flux are important, and their relative importance varies with both altitude and, importantly, from one subregion of the storm to the next. While this complexity presents a significant and daunting challenge for parameterizing momentum tendencies by squall lines in large-scale prediction and climate models, the well-defined and repeatable structure of squall lines with trailing stratiform precipitation (e.g., Houze et al. 1990) of the storm increases the tractability of the problem.

Acknowledgments. The guidance from Professor R. A. Houze, Jr. is highly appreciated. Scott Braun, David Kingsmill, Peggy LeMone, Tom Matejka, and Sandra Yuter provided very helpful comments and suggestions. This research was supported by NSF Grant ATM-9409988 in USA.

REFERENCES

Biggerstaff, M. I., and R. A. Houze, Jr., 1993: Kinematics and microphysics of the transition zone of the 10-11 June 1985 squall line. *J. Atmos. Sci.*, **50**, 3091–3110.

Caniaux, G., J.-P. Lafore, and J.-L. Redelsperger, 1995: A numerical study of the stratiform region of a fast-moving squall line. Part II: Relationship between mass, pressure, and momentum fields. *J. Atmos. Sci.*, **52**, 331–352.

Churchill, D. D., and R. A. Houze, Jr., 1984: Development and structure of winter monsoon cloud clusters on 10 December 1978. *J. Atmos. Sci.*, **41**, 933–960.

Gallus, W. A., Jr., and R. H. Johnson, 1992: The momentum budget of an intense midlatitude squall line. *J. Atmos. Sci.*, **49**, 422-450.

Gao, K., D.-L. Zhang, M. W. Moncrieff, and H.-R. Cho, 1990: Mesoscale momentum budget in a midlatitude squall line: A numerical case study. *Mon. Wea. Rev.*, **118**, 1011-1028.

Houze, R. A., Jr., 1982: Cloud clusters and large-scale vertical motions in the tropics. *J. Meteor. Soc. Japan*, **60**, 396–410.

———, 1989: Observed structure of mesoscale convective systems and implications for large-scale heating. *Quart. J. Roy. Meteor. Soc.*, **115**, 425–461.

———, 1993: Cloud Dynamics. *Academic Press*, 573 pp.

———, B. F. Smull, and P. Dodge, 1990: Mesoscale organization of springtime rainstorms in Oklahoma. *Mon. Wea. Rev.*, **118**, 613-654.

Johnson, R. H., and P. J. Hamilton, 1988: The relationship of surface pressure features to the precipitation and the air-flow structure of an intense midlatitude squall line. *Mon. Wea. Rev.*, **116**, 1444-1472.

Klemp, J. B., and R. B. Wilhelmson, 1978: The simulation of three-dimensional convective storm dynamics. *J. Atmos. Sci.*, **35**, 1070-1096.

LeMone, M. A., 1983: Momentum flux by a line of cumulonimbus. *J. Atmos. Sci.*, **40**, 1815-1834.

———, and M. W. Moncrieff, 1994: Momentum and mass transport by convective bands: Comparisons of highly idealized dynamical models to observations. *J. Atmos. Sci.*, **51**, 281–305.

———, G. M. Barnes, and E. J. Zipser, 1984: Momentum flux by lines of cumulonimbus over tropic oceans. *J. Atmos. Sci.*, **41**, 1914-1932.

Mapes, B. E., and R. A. Houze, Jr., 1995: Diabatic divergence profiles in western Pacific mesoscale convective systems. *J. Atmos. Sci.*, **52**, 1807-1828.

Moncrieff, M. W., 1981: A theory of organized steady convection and its transport properties. *Quart. J. Roy. Meteor. Soc.*, **107**, 29-50.

———, 1992: Organised mesoscale convective systems: archetypal dynamical models, mass and momentum flux theory, and parameterization. *Quart. J. Roy. Meteor. Soc.*, **118**, 819-850.

Priestly, C. H. B., 1949: Heat transport and zonal stress between latitudes. *Quart. J. Roy. Meteor. Soc.*, **75**, 28–40.

Rutledge, S. A., and R. A. Houze, Jr., M. I. Biggerstaff, and T. Matejka, 1988: The Oklahoma-Kansas mesoscale convective system of 10-11 June 1985: Precipitation structure and single-Doppler radar analysis. *Mon. Wea. Rev.*, **116**, 1409–1430.

Schneider, E. K., and R. S. Lindzen, 1976: A discussion of the parameterization of momentum exchange by cumulus convection. *J. Geophys. Res.*, **81**, 3158-3161.

Skamarock, W. C., M. L. Weisman, and J. B. Klemp, 1994: Three-dimensional evolution of simulated long-lived squall lines. *J. Atmos. Sci.*, **51**, 2563–2584.

Steiner, M., R. A. Houze, Jr., and S. E. Yuter, 1995: Climatological characterization of three-dimensional storm structure from operational radar and rain gauge data. *J. Appl. Meteor.*, **34**, 1978-2007.

Stevens, D. E., R. S. Lindzen, and L. J. Shapiro, 1977: A new model of tropical waves incorporating momentum mixing by cumulus convection. *Dyn. Atmos. Oceans.*, **1**, 365-425.

Yang, M.-J., and R. A. Houze, Jr., 1995a: Multicell squall line structure as a manifestation of vertically trapped gravity waves. *Mon. Wea. Rev.*, **123**, 641–661.

———, and ———, 1995b: Sensitivity of squall-line rear inflow to ice microphysics and environmental humidity. *Mon. Wea. Rev.*, **123**, 3175-3193.

Zhang, D.-L., K. Gao, and D. B. Parsons, 1989: Numerical simulation of an intense squall line during 10-11 June 1985 PRE-STORM. Part I. Model verification. *Mon. Wea. Rev.*, **117**, 960-994.

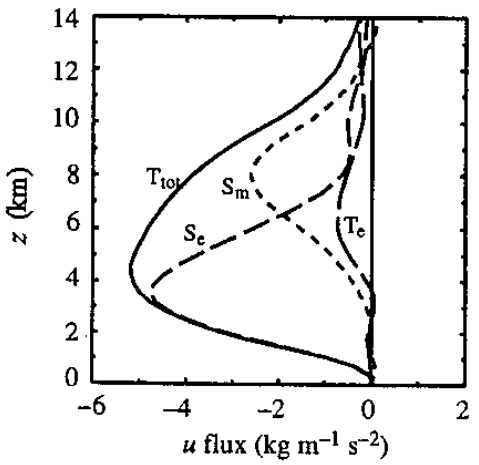

Figure 1. Total vertical flux of storm-relative momentum (T_{tot}) and its three components—the transports by the steady mean flow (S_m), standing eddies (S_e), and transient eddies (T_e)—over the large-scale area A during the mature stage (t = 10–11 h).

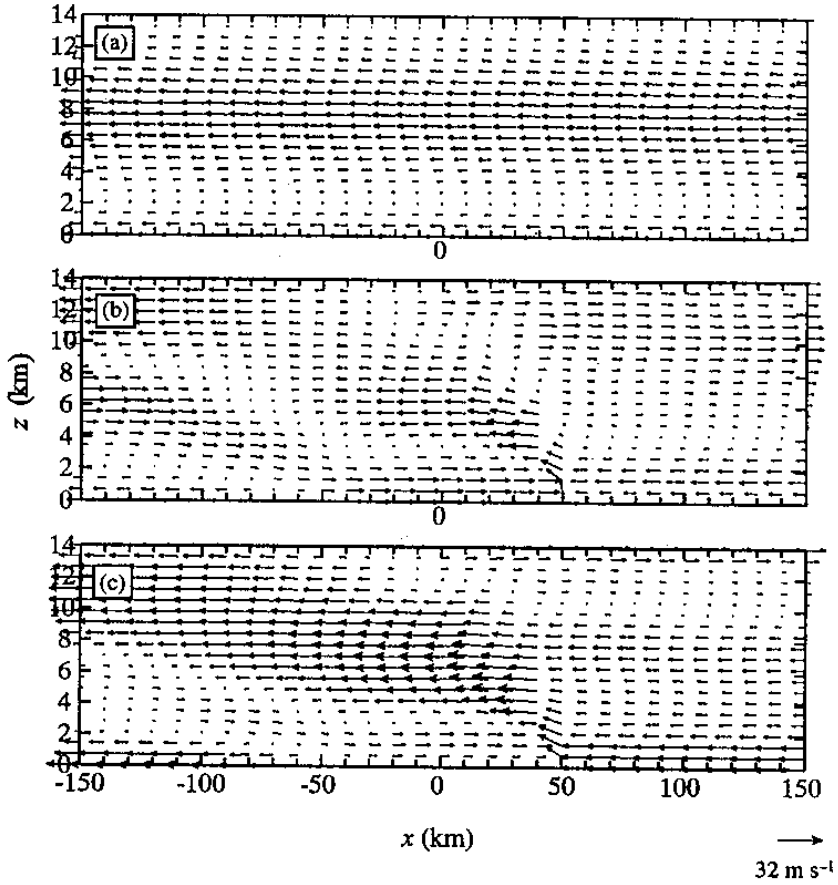

Figure 2 . Vertical cross section of vectors of (a) domain-averaged wind ($[\overline{u_s}]$, $[\overline{w}]$), (b) standing eddy ($\overline{u_s}^*$, $\overline{w}^*$), and (c) total wind ($\overline{u_s}$, $\overline{w}$) during the mature stage (t = 10-11 h) of the storm.

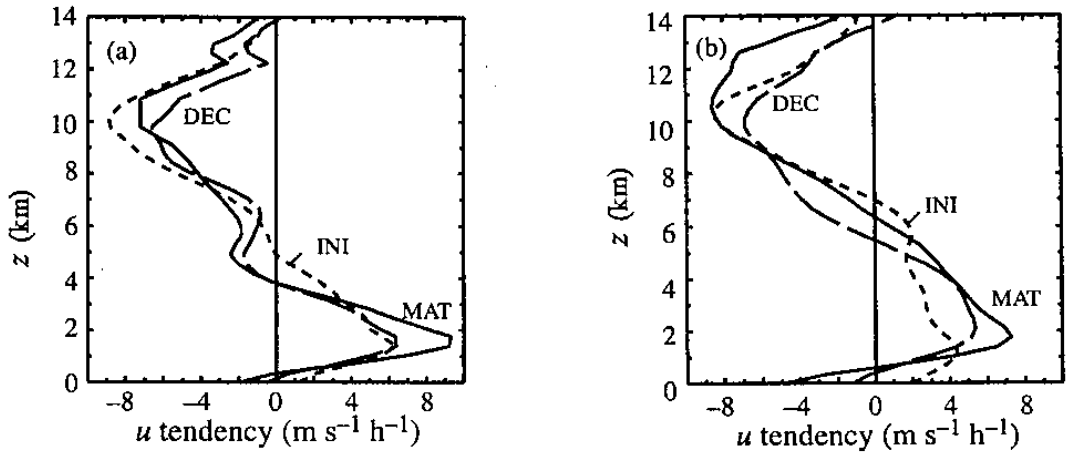

Figure 3. (a) Left-hand and (b) right-hand side of equation (6) for the initial (INI; t = 7.5–8.5 h), mature (MAT; t = 10–11 h), and slowly decaying (DEC; t = 12.5–13.5 h) stages of the storm.

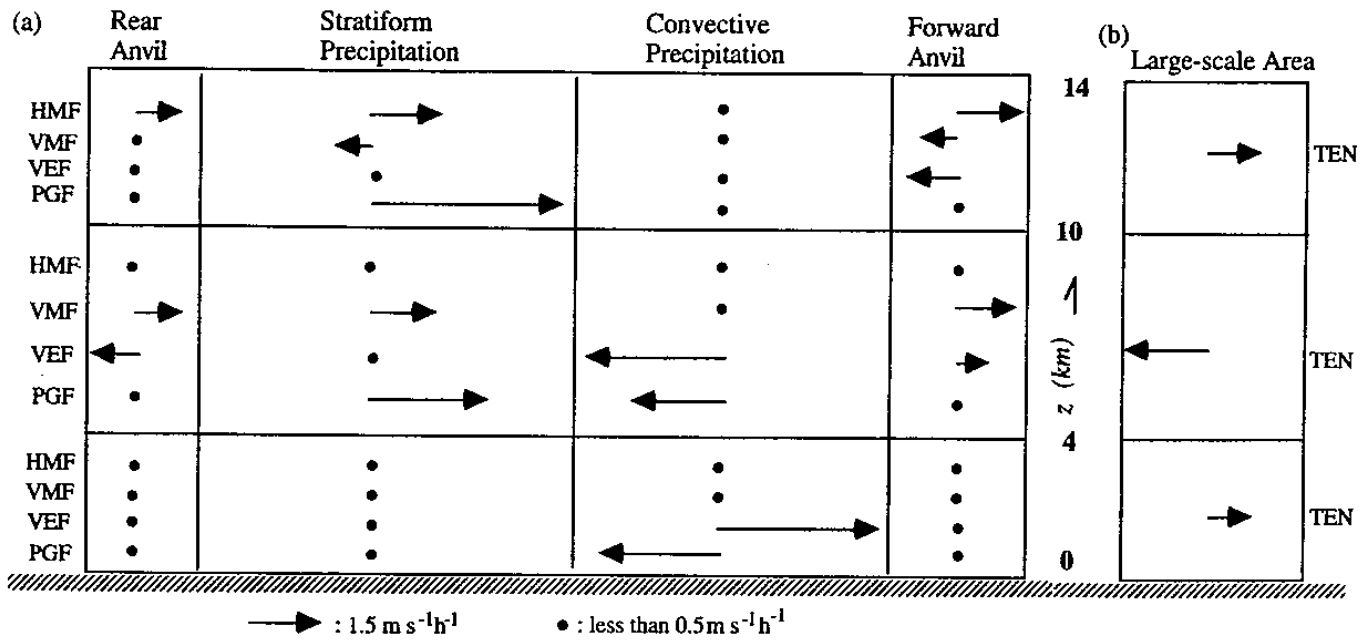

Figure 4 (a) A block diagram showing the balance of area-weighted momentum-budget terms in (8) over four subregions of a large-scale area during the mature stage of the simulated 10-11 June 1985 squall line. Rightward-pointing arrow is for positive (rear-to-front) u-tendency and leftward-pointing arrow is for negative (front-to-rear) u-tendency. The length of arrow is proportional to the layer-averaged tendency produced by each budget term. A dot is for tendency less than 0.5 m s^{-1} h^{-1}. Panel (b) is the same as (a) except for net momentum tendency, the term on the left-hand side of (8), over the total 300-km-wide large-scale area.